IEEE Access
Multidisciplinary | Rapid Review | Open Access Journal

Received August 11, 2019, accepted September 5, 2019, date of publication September 10, 2019,
date of current version September 25, 2019.

Digital Object Identifier 10.1109/ACCESS.2019.2940587

Femtosecond Pulse Temporal Overlap Estimation and Adjustment in SSFS-Based CARS System

YONGNING ZHANG[1,2,3], JUNFENG JIANG[1,2,3], SHUANG WANG[1,2,3], KUN LIU[1,2,3], ZHE MA[1,2,3], GAOFEI GU[1,2,3], RONGQING HUI[4], AND TIEGEN LIU[1,2,3]

[1]School of Precision Instruments and Opto-electronics Engineering, Tianjin University, Tianjin 300072, China
[2]Tianjin Optical Fiber Sensing Engineering Center, Institute of Optical Fiber Sensing, Tianjin University, Tianjin 300072, China
[3]Key Laboratory of Opto-electronics Information Technology, Tianjin University, Tianjin 300072, China
[4]Department of Electrical Engineering and Computer Science, The University of Kansas, Lawrence, KS 66045, USA

Corresponding author: Junfeng Jiang (jiangjfjxu@tju.edu.cn)

This work was supported in part by the National Natural Science Foundation of China under Grant 61735011, Grant 61675152, Grant 61378043, Grant 61475114, and Grant 61505139, in part by the National Instrumentation Program of China under Grant 2013YQ030915, in part by the Open Project of Key Laboratory of Opto-electronics Information Technology under Grant 2018KFKT013, and in part by the First Rank of Tianjin 131 Innovation Talent Development Program.

ABSTRACT We present and verify a residual-pump-based temporal overlap estimation method in soliton self-frequency shift-based coherent anti-Stokes Raman scattering system. The residual pump light, output by a highly nonlinear photonic crystal fiber, acts as a crucial link between the pump and Stokes pulses during the temporal overlap estimation. The wavelength-dependent optical delay is estimated to be 0.141 ps/nm when the Stokes wavelength is 900 nm $\sim$ 1050 nm according to the temporal overlap estimation method. The actual measurement result is 0.138 ps/nm based on the nonresonant signal from a microscope slide, which is very close to the estimated result. In addition, the Raman resonant signals of liquid cyclohexane at 2853 cm^{-1}, 2923 cm^{-1} and 2938 cm^{-1} have also been successfully detected at the predicted optical delays 427.27 ps and 428.17 ps.

INDEX TERMS Fiber nonlinear optics, optical solitons, interference, Raman scattering, CARS, GNLSE.

I. INTRODUCTION

Coherent anti-Stokes Raman scattering (CARS) technology has attracted many attentions in recent years as it maps the targeted molecular in the sample by probing its vibrational information in a non-invasive and label-free manner [1]–[3]. S. Osseiran *et. al.* explored the melanin species and their drug reactions by CARS microscopy [4]. S. You *et. al.* tried to explain the role of docosanol in herpes simplex labialis treatment by intracellular imaging of CARS microscopy [5]. C. C. Moura *et. al.* introduced the application of CARS in skeletal cells and skeletal regeneration [3]. CARS technology is based on the nonlinear four-wave mixing process, which is coherently driven when the energy level difference between pump pulses and Stokes pulses resonates with a Raman active molecular transition [6]. The CARS signal is enhanced greatly by the actively molecular resonance compared to the spontaneous Raman scattering, meanwhile the spectrally blue-shifted CARS signal is easily detected without the influence of one-photon fluorescence background which provides a high signal noise ratio [2]. The third-order nonlinear effects can be generated only in a small volume of focus, which make CARS an inherently three-dimensional tomography. Owing to the advantages above, CARS technology is very useful in non-invasive imaging of living cells [7], protein structure [8], lipid membranes [9] and so on [10], [11].

So far, many techniques, such as time-resolved [12], [13], polarization-control [14], coherent-control [15], Fourier-transform technology [16], [17], frequency-modulation technology [18], dual-comb technology [19], have been proposed to improve the performance of CARS system. Soliton self-frequency shift (SSFS) effect have attracted some researchers' attentions due to the advantages of simple structure, low cost and convenient wavelength tuning [20]–[22]. In SSFS-based CARS systems, temporal overlap is a critical step so that the pump and Stokes pulses can interacted with the molecular vibration simultaneously. An optical delay line or a motorized delay stage is usually used to change the relative optical delay between the pump and Stokes pulses. As the full width of half maximums (FWHMs) of the pump

The associate editor coordinating the review of this manuscript and approving it for publication was Derek Abbott.

and Stokes pulses are usually a few hundred femtoseconds or a few picoseconds, it is almost impossible to observe the temporal overlap directly by an oscilloscope. In addition, the wavelength-dependent delay, which is caused by the walk-off effect of ultrashort pulses corresponding to different wavelengths, makes the adjustment of temporal overlap spend more time in SSFS-based CARS systems [23], [24]. When a complete Raman resonance spectrum of the sample is measured in SSFS-based CARS system, the Stokes wavelength is scanned and the relative optical delay between pump and Stokes is also changed continuously due to the wavelength-dependent delay. Thus, the optical delay should be adjusted synchronously with the Stokes wavelength tuning to ensure the temporal overlap over the whole Raman spectral measurement. Therefore, the optical delay line is adjusted frequently when different Raman resonances are detected in SSFS-based CARS system. However, there is little literature to discuss temporal overlap control and the optical delay is still confirmed by the excitation signals of standard materials, which means that the temporal overlap needs more time during the Raman spectral measurement in SSFS-based CARS system. In addition, the sum-frequency generation is also inconvenient for temporal overlap estimation in SSFS-based CARS system because of the limited optical power and phase-match. Thus, the temporal overlap, influenced by the wavelength-dependent delay, prevents SSFS-based CARS system from becoming an efficient automated tool.

In this letter, a temporal overlap estimation method in SSFS-based CARS system is presented and verified, which takes full use of the residual pump light in the highly nonlinear photonic crystal fiber (PCF) as a crucial link. The optical delay needed for temporal overlap is divided into two parts: the dispersion delay and the optical-path delay. Firstly, the dispersion delay between the Stokes pulse and the residual pump in the highly nonlinear PCF is calculated by the general nonlinear Schrödinger equation (GNLSE). Secondly, the optical-path delay between the pump pulse and the residual pump is measured by interference spectra. At last, the synthetic optical delay needed for temporal overlap can be estimated based on the two optical delays above. Although the interference spectrum is a common phenomenon in optical field, it is rare to be used in SSFS-based CARS system because the residual pump output by the PCF is usually ignored. In addition, the wavelength-dependent delay of the Stokes pulse needs an effective method to ensure the temporal overlap over the whole tuning range of Stokes wavelength. Based on the temporal overlap estimation method propose by us, the optical delay needed for temporal overlap in the whole tuning range of Stokes wavelength can be obtained by only one calculation and measurement. Compared with the optical delay calibration method based on Raman resonances of standard samples which is usually used in laboratories, the temporal overlap estimation method proposed by us has advantages of wide wavelength suitability, flexible PCF change and quick troubleshooting capability in SSFS-based CARS system. The proposed method simplifies the temporal overlap adjustment and helps to realize a dynamical closed-loop feedback time delay control, which will be useful for an effectively and reliably automate temporal overlap control of ultrashort pulses in SSFS-based CARS system.

II. PRINCIPLE

Figure 1 shows the schematic diagram of the residual-pump-based temporal overlap estimation method in SSFS-based CARS system. Femtosecond pulse acts as the system's light source and is divided into two parts: one part is injected into a highly nonlinear PCF to generate optical solitons by SSFS effect and the fundamental soliton serves as the Stokes pulse; the other part serves as the pump pulse. The temporal walk-off or the optical delay τ between the pump and Stokes pulses can be divided into two parts, the dispersion delay τ_1 and the optical-path delay τ_2, namely $\tau = \tau_1 + \tau_2$. The dispersion delay τ_1 between the fundamental soliton and the residual pump is caused by chromatic dispersion and nonlinearity of the highly nonlinear PCF, and it can be calculated by the GNLSE. The optical-path delay τ_2 between the pump pulse and the residual pump is caused by the physical optical path difference between the pump and Stokes paths. It can be measured by the interference spectra between the residual pump and the pump pulse. The time delay of the optical delay line in pump path is defined as the compensated time delay τ_c and it will be scanned. When the pump pulse moves to the position shown by the blue dashed line by scanning the optical delay line ($\tau_c = \tau_2$), obvious spectrum interference can be observed. When the compensated time delay τ_c is equal to optical delay τ, the pump pulse moves to the position shown by the blue dotted line and meets the Stokes pulse, and the temporal overlap is realized in CARS system.

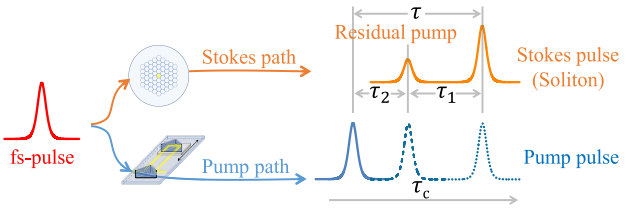

FIGURE 1. Schematic diagram of residual-pump-based CARS femtosecond pulse temporal overlap estimation.

At first, the dispersion delay τ_1 between optical soliton and residual pump in the highly nonlinear PCF is calculated by the GNLSE [25].

$$\frac{\partial A}{\partial z} = -\frac{\alpha}{2}A - \frac{i\beta_2}{2}\frac{\partial^2 A}{\partial T^2} + \frac{\beta_3}{6}\frac{\partial^3 A}{\partial T^3} + i\gamma\left[|A|^2 A + \frac{i}{\omega_0}\frac{\partial}{\partial T}\left(|A|^2 A\right) - T_R\frac{\partial |A|^2}{\partial T}A\right], \quad (1)$$

$$T = t - z/v_g, \quad t \ni \tau_1. \quad (2)$$

where, A is the light wave amplitude, z is the propagation distance, β_2 is the fiber second-order dispersion, β_3 is the

fiber third-order dispersion, α is the fiber loss, γ is the fiber nonlinearity, T_R is the Raman response, ω_0 is the frequency corresponding to center wavelength of injected light, T is the time variable of moving coordinates, and v_g is the group velocity.

Then, the optical-path delay τ_2 can be identified by the oscillation's magnitude of interference spectra [26]:

$$I(\lambda, \tau) = 4\left[\cos\left(\frac{\pi c \tau}{\lambda}\right)\right]^2 \cdot I_0(\lambda), \tag{3}$$

$$\tau_2 = \tau\left(\max\left[\int \left|I(\lambda, \tau) - I_{ref}(\lambda, \tau)\right| d\lambda\right]\right). \tag{4}$$

where, $I(\lambda, \tau)$ is the intensity of interference spectra, the spectra of pump pulse and residual pump pulse are simplified assumed to be the same and represented by $I_0(\lambda)$, $I_{ref}(\lambda, \tau)$ represents the reference interference spectra when the pump pulse and residual pump pulse are away from each other.

III. MEASUREMENT AND DISCUSSION

A. EXPERIMENTAL SETUP

Figure 2 shows the experimental setup of our CARS system and the characteristics of the femtosecond pulse. As presented in Fig. 2(a), the horizontally polarized femtosecond pulse, generated by the femtosecond laser source, transfers through a liquid crystal variable retarder (LCVR) and a polarizing beam splitter (PBS). By adjusting the voltage of the LCVR, the polarization of the femtosecond pulse can be rotated. The power ratio of two orthogonally polarized pulses output by the PBS can be continuously and rapidly adjusted. On the one hand, the horizontally polarized femtosecond pulse is injected into a 2.86 m highly nonlinear PCF (NKT, NL-PM-750) to generate optical solitons by SSFS effect. The fundamental soliton passes through a 30 cm SF10 glass rod and serves as the Stokes pulse. On the other hand, the vertically polarized femtosecond pulse from the PBS passes through an optical delay line (ODL) and a 20 cm SF10 glass rod, and then acts as the pump pulse. SF10 glass rods are used to introduce linear chirps to the pump and Stokes pulses to enhance the spectral resolution based on spectral focusing [27]–[29]. The temporal widths of the linearly chirped pump and Stokes pulses are around 1450 fs and 1100 fs calculated by the GNLSE and the chromatic dispersion of SF10 glass rods. A long-pass dichroic mirror (DMLP, cutoff wavelength of 900 nm) is used to combine the pump and Stokes pulses. The reflection part of the Stokes pulse and transmission part of the pump pulse are detected by an optical spectrum analyzer (OSA, Ocean Optics, HR4000+) to analyze the interference spectra as the ODL scanning. The transmission part of the Stokes pulse and the reflection part of the pump pulse are focused by a focusing microscope objective (L1, Nikon, 20X, numerical aperture of 0.5) to liquid cyclohexane. Another same microscope objective (L2) collects the excitation signal of cyclohexane. Then, the excitation signal passes through two short-pass filters (F2, cutoff wavelength of 750 nm) for optimizing the CARS signal and filtering out the pump and Stokes pulses. At last, the optimized signal is detected by a photomultiplier tube (PMT, Thorlabs, PMM02). Figure 2(b) shows that the FWHM of the femtosecond pulse autocorrelation trace is 124.20 fs, which means that the FWHM of the actual hyperbolic secant pulse is 80.49 fs. Figure 2(c) indicates that the FWHM of the femtosecond pulse spectrum is 12.82 nm and the center wavelength is 783 nm.

The optical spectrum evolution of optical solitons is presented in Fig. 3(a). The center wavelength of the fundamental soliton increases approximately linearly and the maximum

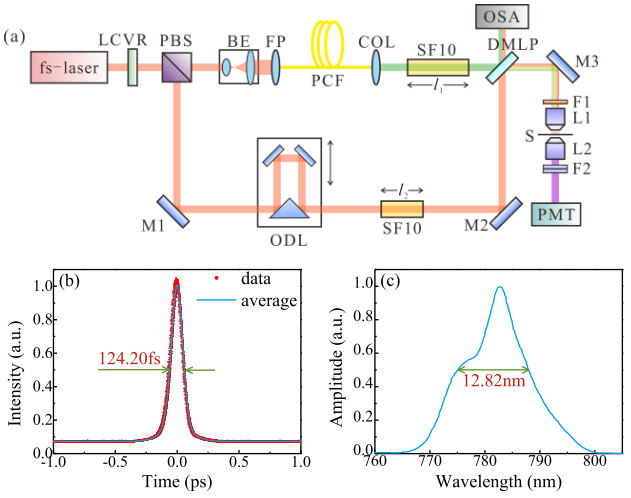

FIGURE 2. (a) Experimental setup for CARS system. LCVR: liquid crystal variable retarder, PBS: polarizing beam splitter, BE: beam expander, FP: fiber-port, PCF: photonic crystal fiber, COL: collimator lens, SF10: SF10 glass rod, l_1 = 30cm, l_2 = 20cm, DMLP: long-pass dichroic mirror, M1, M2, M3: reflector mirrors, ODL: optical delay line, F1: long-pass filter, F2: short-pass filter, L1, L2: objective lenses, S: sample, OSA: optical spectrum analyzer, PMT: photomultiplier tube. (b) Autocorrelation trace of femtosecond pulse. (c) Optical spectrum of femtosecond pulse.

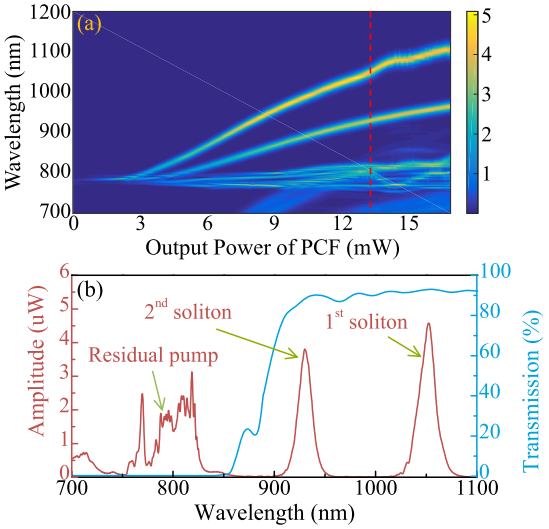

FIGURE 3. (a) Optical soliton evolution versus output power of PCF. (b) Optical spectrum at fundamental soliton's wavelength 1050 nm (red trace) and transmission of the DMLP (blue trace).

value is nearly 1100 nm. Thus, the maximum wavenumber which can be detected based on our SSFS-based CARS system is about 3680 cm^{-1} when the center wavelength of the pump pulse is 783 nm. The red dashed line in Fig. 3(a) indicates that the center wavelength of fundamental soliton is 1050 nm, and the detailed optical spectrum is presented in Fig. 3(b) by the red trace. According to the detailed optical spectrum, the center wavelengths of fundamental and second solitons are 1050 nm and 930 nm, respectively. The residual pump of the highly nonlinear PCF is also clearly shown in Fig. 3(b). Although the optical spectrum of the residual pump is different from the original spectrum in the spectral shape and phase, it remains stability when the interference spectra between the residual pump and the pump pulse are measured by scanning the relative optical delay and this is enough for the optical-path delay measurement. Therefore, the spectral shape and phase of the residual pump have little effect on the interference spectra as long as the initial reference spectrum is chosen. The blue trace in Fig. 3(b) shows transmission of the DMLP used in our experiment. It indicates that the optical spectrum above 900 nm will be mostly transmitted, however the spectrum below 850 nm will be blocked mostly. The transmission part of the pump pulse through the DMLP is usually weak and ignored, but here it acts as a critical link during the temporal overlap estimation method proposed by us. The interference spectra between the residual pump and the transmission part of the pump pulse through the DMLP is used to defined the optical-path delay τ_2.

B. CALCULATION OF THE DISPERSION DELAY

At first, the dispersion delay is calculated by the GNLSE and the result is presented in Fig. 4. The PCF's parameters used in our CARS system are set as following: $z = 2.86$ m, $\alpha = 0.05$ dB/m, $\gamma = 0.095$ W^{-1} m^{-1}, $\beta_2 = -6.90 \times 10^{-27}$ s^2/m, $\beta_3 = -6.04 \times 10^{-41}$ s^3/m, $T_R = 3$ fs, $\omega_0 = 384.62$ THz. The pump pulse of the highly nonlinear PCF is the hyperbolic secant pulse without initial chirp, and the FWHM duration is 80.49 fs. Figures 4(a) and 4(b) indicate that the time domain and optical spectrum when the center wavelength of fundamental soliton is 800 nm, and the relative optical delay, namely the dispersion delay, between the fundamental soliton and the injected pulse is 0.24 ps. Figure 4(c) and 4(d) show the same as above when the center wavelength increases to 1050 nm, and the dispersion delay raises to 27.26 ps correspondingly. Figure 4(e) shows that the change of the dispersion delay when the center wavelength of fundamental soliton increases from 800 nm to 1050 nm. The dispersion delay increases nonlinearly from 0.24 ps to 27.26 ps over the whole tuning range of soliton's wavelength.

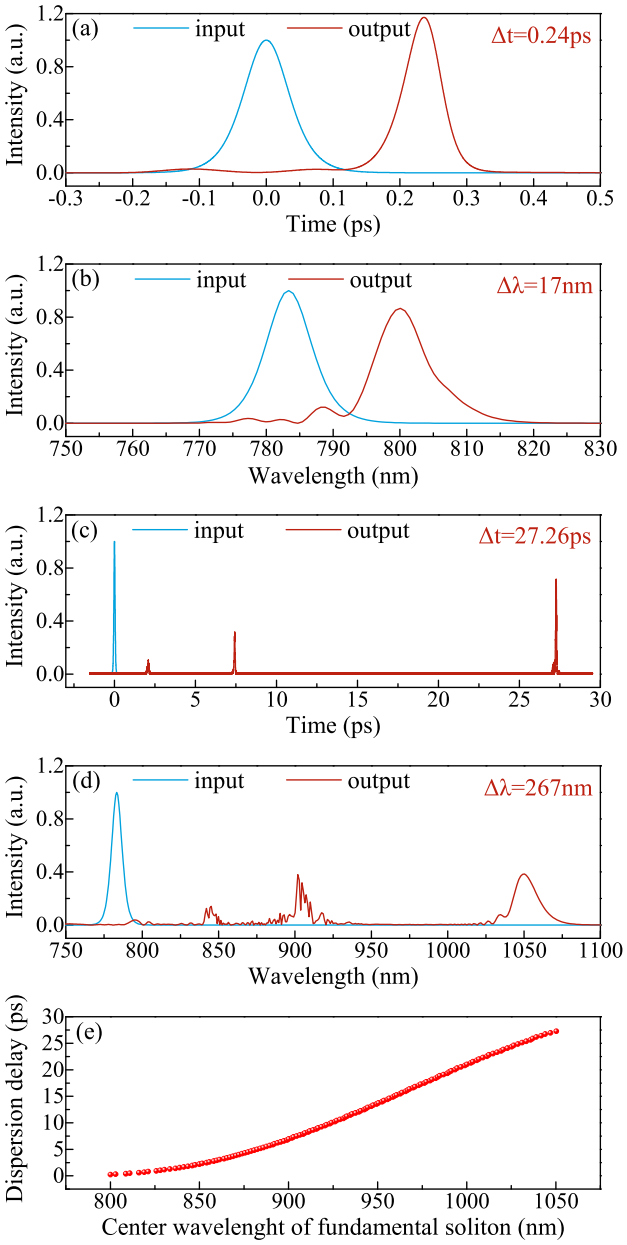

FIGURE 4. (a) and (b) Time domain and optical spectrum at fundamental soliton's wavelength 800 nm. (c) and (d) The same as above at fundamental soliton's wavelength 1050 nm. (e) Relationship between the dispersion delay and fundamental soliton's wavelength.

C. MEASUREMENT OF THE OPTICAL-PATH DELAY

Secondly, the optical-path delay is measured by analyzing the interference spectra. The interference spectra at different optical delays is presented in Fig. 5. When the optical delay is 0 ps, the optical spectrum around 783 nm is smooth and it is similar with the spectrum in Fig. 2(c), which means that there is no optical spectrum interference. Whereas, when the optical delay increases from 0 ps to about 175 ps, some wrinkles appear on interference spectra at first and then the oscillation of interference spectra becomes more and more obvious. After the maximum oscillation, the interference spectra return to smooth gradually when the optical delay increases continuously. The evolution of interference spectra indicates that the optical path difference between the pump and Stokes paths decreases to zero at first and then increases. The optical delay, corresponding the maximum oscillation of

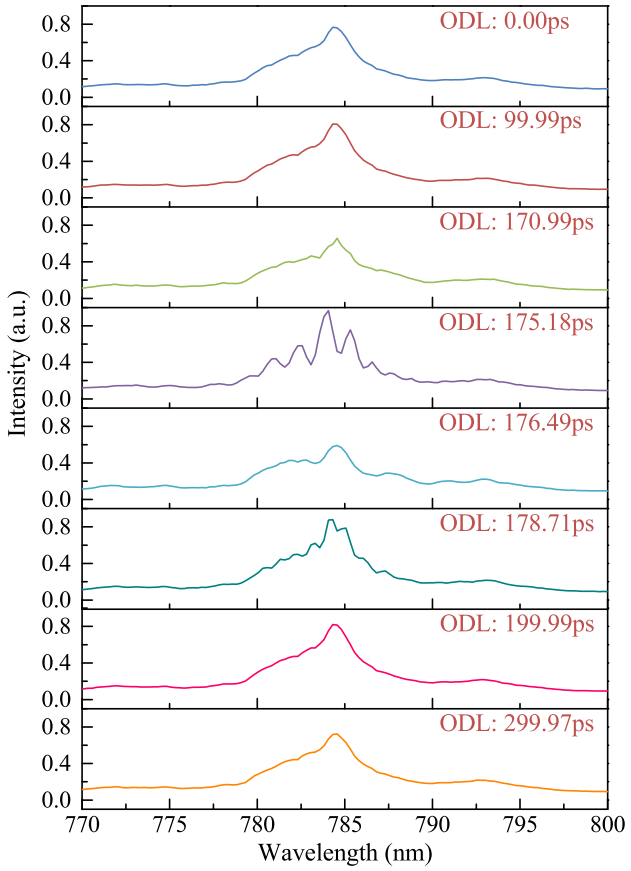

FIGURE 5. Interference spectra at different optical delays.

interference spectra, means that the residual pump in Stokes path and the pump pulse in pump path meet each other.

Based on the interference spectra and Eq. (3), the optical-path delay can be identified. Figure 6(a) shows the oscillation's magnitude of the interference spectra when the optical delay increases from 0 ps to 300 ps in steps of 0.01 ps. The oscillation's magnitude culminates at the optical delay of 176.52 ps, which means that the optical distance of pump path is equal to that of Stokes path in our CARS system. It is worth noting that there is a sub-peak on the left side of the main-peak, and it is ascribed to the secondary reflection of the DMLP. The measurement result in Fig. 6(a) also proves that the spectral shape and phase of the residual pump in Fig. 3(b) have little effect on the interference spectra and the demodulation method of interference spectra is effective enough to determine the optical-path delay. We carried out ten measurements, and the measurement result of the optical-path delay is 176.55±0.05 ps (namely $\tau_2 = 176.55 \pm 0.05$ ps), as shown in Fig. 6(b).

Figure 6(c) shows time sequence of the pump pulse detected by a photodetector (bandwidth 1 GHz) and an oscilloscope (sampling rate 40 GS/s) directly. Obviously, due to the limited bandwidth and sampling rate, the time sequence has a long tail and the FWHM is around 1.50 ns, which can't indicate the actual pulse shape. Here, the peak position of the pump pulse's time sequence is used to indicate the

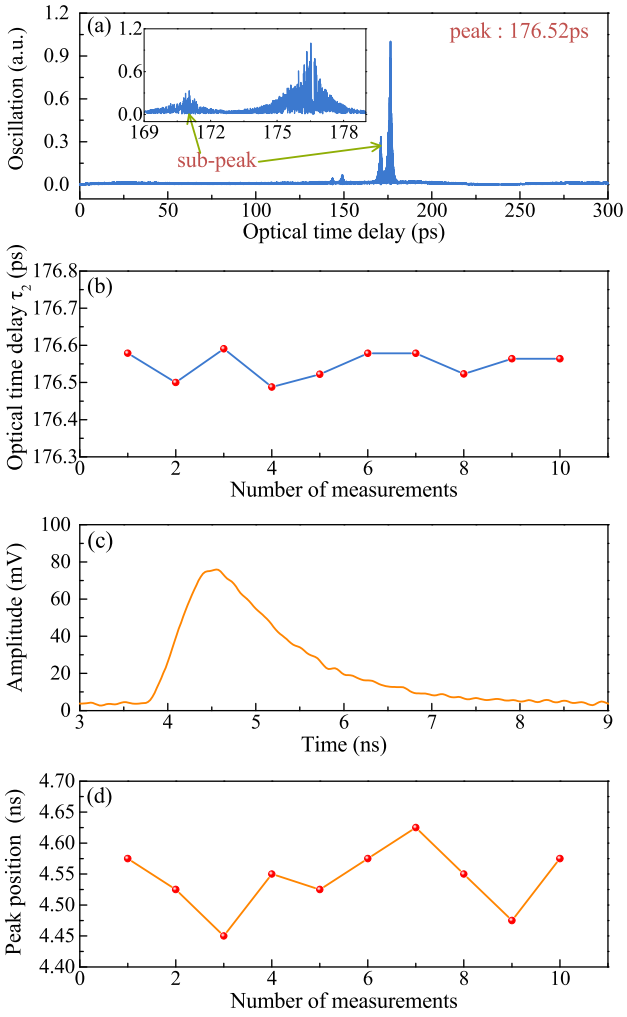

FIGURE 6. (a) Oscillation's magnitude versus optical delay. (b) Ten measurements of τ_2. (c) Time sequence of pump pulse measured directly. (d) Ten measurements of the peak position, when the central wavelength of fundamental soliton is 1050 nm.

time-position in time domain. The fluctuation range of the time trace's peak position represents the inaccuracy of the pump pulse's time-position, which is directly related to the adjustment range of the optical delay line in the pump path. Figure 6(d) shows ten measurements results of the time trace's peak position of the pump pulse, and the fluctuation range is ±87.50 ps, which means that the scan range of the optical delay line is at least 175 ps to realize temporal overlap between the pump and Stokes pulses. Compared to the fluctuation range ±0.05 ps of the optical-path delay measured by interference spectra, the directly measurement result is imprecise. Thus, the temporal overlap in CARS system is usually a time-wasting process, especially for the adjustment of wavelength-dependent propagation delay in the soliton-based Stokes path.

D. SYNTHETIC OPTICAL DELAY AND VERIFICATION

Based on the dispersion delay and the optical-path delay above, the synthetic optical delay needed for temporal overlap

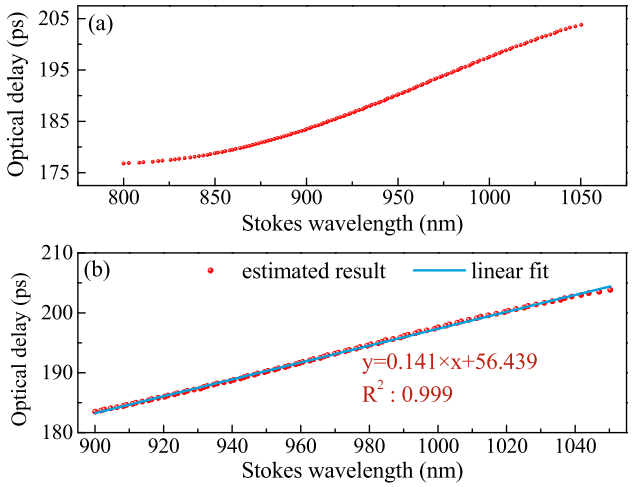

FIGURE 7. (a) Synthetic relative optical delay. (b) Linear fit of the synthetic relative optical delay at Stokes wavelength 900 nm ∼ 1050 nm.

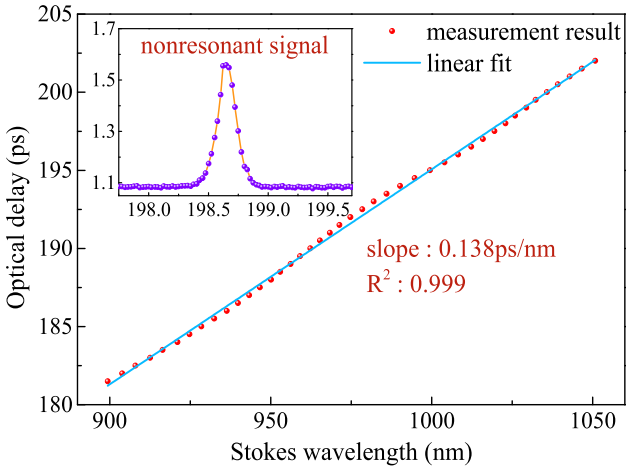

FIGURE 8. Optical delay of the nonresonant signal versus Stokes wavelength.

can be estimated and the result is presented in Fig. 7. When the center wavelength of the Stokes pulse increases from 800 nm to 1050 nm, the synthetic optical delay is estimated to raise from 176.79 ps to 203.81 ps and the estimated accuracy is ±0.05 ps, determined by the optical-path delay. The error of synthetic optical delay is dominated by the measurement of the optical-path delay, and absolute on-axis accuracy and step size of the optical delay line are the direct causes of measurement error. The dependence of synthetic optical delay on Stokes wavelength is nonlinear over the whole Stokes wavelength. Nevertheless, the synthetic optical delay increases approximately linearly when the Stokes wavelength is 900 nm ∼ 1050 nm. For the data analysis and comparison, the linear fitting of the optical delay when the Stokes wavelength is greater than 900nm is used to verified the accuracy of the proposed temporal overlap estimation method. Figure 7(b) shows the linear fit of the estimated optical delay when Stokes wavelength is between 900 nm and 1050 nm. The linear fit indicates that the synthetic optical delay is estimated to be increased by 0.141 ps in our SSFS-based CARS system when Stokes wavelength increases by 1 nm from 900 nm to 1050 nm.

In order to verify the proposed temporal overlap estimation method, the nonresonant signal from a microscope slide [30], [31] at different Stokes wavelengths is measured and the result is presented in Fig. 8. Due to the cutoff wavelength 900 nm of the DMLP, the nonresonant signal is measured when the Stokes wavelength is over 900 nm. In order to compared with the estimated synthetic optical delay directly, the SF10 glass rods are removed from the SSFS-based CARS system when the nonresonant signal is measured. The illustration in Fig. 8 shows the nonresonant signal changes as the optical delay scanning between 197.50 ps and 199.75 ps when the Stokes wavelength is 1030 nm. Obviously, the optical delay at the signal's peak indicates the temporal overlap in our CARS system. When the center wavelength of Stokes pulse increases from around 900 nm to 1050 nm, the optical delay of the nonresonant signal raises linearly with a slope of 0.138 ps/nm, which is a little smaller than the estimated result 0.141 ps/nm. The difference between the estimated result and the measurement result may be caused by the chromatic dispersion of optical devices in the Stokes path which is not calculated in the estimated result.

In addition, the C-H band of liquid cyclohexane has also been used as the sample to further verify the temporal overlap estimation method in the SSFS-based CARS system. In order to make a balance between the energy of ultrashort pulses and the spectral resolution of Raman measurement, a suitable linear chirp is introduced to the pump and Stokes pulses by passing through the SF10 glass rods. The suitable linear chirp enhances the Raman spectral resolution by spectrum focusing [28], [29], and does not cause a large waste of the pulse energy. Here, the average optical powers of the pump and Stokes pulses are about 0.90 mW and 0.45 mW and the temporal widths of the linearly chirped pump and Stokes pulses are about 1450 fs and 1100 fs. With the spectral widths of 12.82 nm (pump light) and 16.60 nm (Stokes light), the linearly chirps of the pump and Stokes pulses are around 0.14 cm^{-1}/fs and 0.15 cm^{-1}/fs respectively. The Raman spectral resolution is estimated to be about 13.55 cm^{-1} [23]. The optical delay shift for temporal overlap caused by the SF10 glass rods can be well calculated based on the refractive index of glass, which can be described by the Sellmeier equation $n^2(\lambda) = 1 + \sum_{m=1}^{3} B_m\lambda^2 \Big/ \left(\lambda^2 - C_m\right)$, where the unit of the wavelength is micrometer and the coefficients for SF10 glasses are $(B_1, B_2, B_3) = (1.61626, 0.25923, 1.17491)$ and $(C_1, C_2, C_3) = (0.013607, 0.061596, 121.922710)\ \mu m^2$.

Figure 9(a) shows the adjustment schematic diagram of chirped pulse when the Raman spectrum of cyclohexane is detected. When the Stokes wavelength is λ_1, pump pulse makes temporal overlap with Stokes pulse at optical delay t_1 and Raman shift Ω_1 is detected. If we want to detect the

Raman shift Ω_2, the Stokes wavelength is adjusted to λ_2. Due to the wavelength-dependent optical delay of solitons in SSFS effect, the optical delay should be tuned to t_2 to insure the temporal overlap. Here, the λ_1 and λ_2 are 1008 nm and 1016 nm and the t_1 and t_2 are estimated to be 427.27 ps and 428.17 ps according to the temporal overlap estimation results (198.57 ps and 199.70 ps) in Fig. 7 and the optical delay shifts (228.70 ps and 228.47 ps) caused by the SF10 glass rods. Figure 9(b) shows the spontaneous Raman spectrum of cyclohexane [27] for comparative reference. When the optical delay is adjusted to 427.27 ps and 428.17 ps respectively, the center wavelength of Stokes pulse, satisfying the temporal overlap in our CARS system, are 1008 nm and 1016 nm, corresponding to the resonant wavenumber of 2850 cm^{-1} and 2938 cm^{-1}. By scanning the wavelength of Stokes pulse in range of temporal overlap, the CARS signal of cyclohexane is detected, as shown in Fig. 9(c). When the optical delay is 427.27 ps, the 2853 cm^{-1} resonant Raman spectrum is shown by the red trace. Because of the 2923 cm^{-1} and 2938 cm^{-1} resonant Raman spectra are very close, both of them are detected when the optical delay is adjusted to 428.17 ps, as shown by the blue trace in Fig. 9(c). Due to the larger Stokes wavelength step (around 1.3 nm), determined by the minimum regulating voltage of the LCVR, the CARS signal of cyclohexane is composed of a limited number of data points, and this has a serious influence on the exact position of the Raman spectra, especially for the 2923 cm^{-1} and 2938 cm^{-1} resonant Raman spectra. However, the CARS signal of cyclohexane is very easy to confirm with the two close Raman spectra, and the signal in Fig. 9(c) has been detected over ten times with similar characteristics except for some differences in signal strength. Thus, we confirm that the signal in Fig. 9(c) is the CARS signal of cyclohexane other than nonresonant background noise.

Based on the measurement results of the nonresonant signal from a microscope slide and the CARS signal of cyclohexane, we hold the opinion that the temporal overlap estimation method of combining the dispersion delay and the optical-path delay by the residual pump is usable in SSFS-based CARS system, at least in the 900 nm∼1050 nm range of Stokes wavelengths. Although the slopes of the estimated result (0.141 ps/nm) and the measurement result (0.138 ps/nm) are a little different, the optical delays needed for temporal overlap are estimated to be 427.27 ps and 428.17 ps when the Stokes wavelengths are 1008 nm and 1016 nm respectively, and the corresponding Raman spectra (2853 cm^{-1}, 2923 cm^{-1} and 2938 cm^{-1}) of cyclohexane are still successfully detected. As for the difference between the estimated result in Fig. 7 and the measurement result in Fig. 8, it may be caused by the uncalculated dispersion in the system including collimator lens, long-pass dichroic mirror, long-pass filter, focusing microscope objective and microscope slide. In addition, the dispersion delay based on the GNLSE maybe not accurate enough and more precise parameters of the highly nonlinear PCF are needed. Nonetheless, the temporal overlap between the pump Stokes pulses can be relatively precisely estimated by combining the dispersion delay and the optical-path delay. The result is much better than the direct measurement result detected by a photodetector and an oscilloscope. By this method, we hope that the preparatory work can be greatly reduced and a dynamical closed-loop feedback time delay control for wavelength-dependent propagation system can be realized automatically.

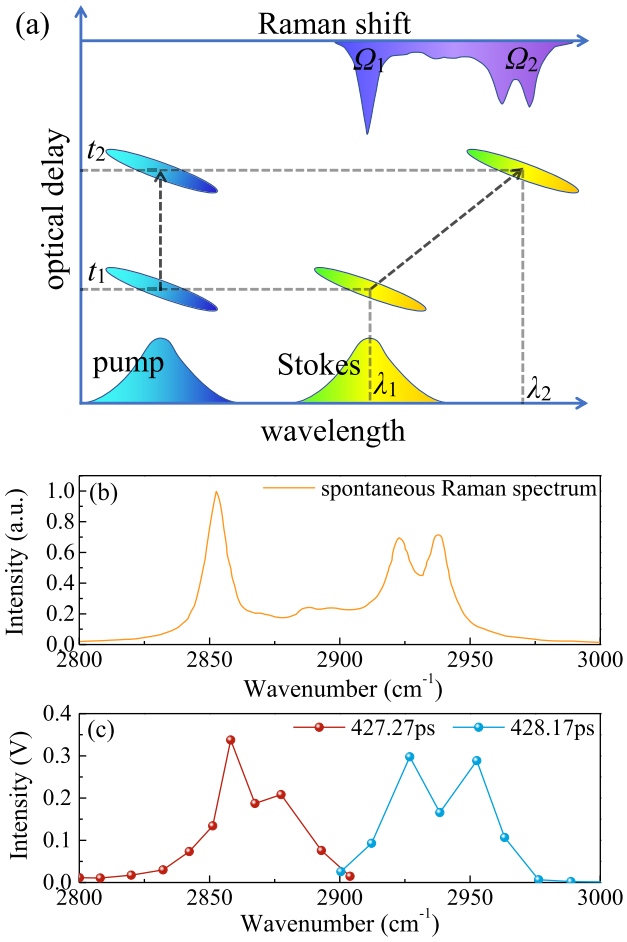

FIGURE 9. (a) Adjustment schematic diagram of chirp pulse, (b) spontaneous Raman spectrum of cyclohexane, (c) measured CARS signal of cyclohexane.

IV. CONCLUSION

In this paper, we propose and demonstrate a residual-pump-based temporal overlap estimation in SSFS-based CARS system. Based on the dispersion delay calculated by the GNLSE and the optical-path delay measured by the interference spectra, the optical delay needed for temporal overlap in our SSFS-based CARS system can be estimated. The nonresonant signal from a microscope slide has been detected when the Stokes wavelength increases from 900 nm to 1050 nm, and the wavelength-dependent optical delay is 0.138 ps/nm, which is slightly less than the estimated result 0.141 ps/nm. The reason maybe the uncalculated dispersion in the Stokes path. The CARS signal of liquid

cyclohexane at 2853 cm^{-1}, 2923 cm^{-1} and 2938 cm^{-1} has also been successfully detected at the estimated optical delay of 427.27 ps and 428.17 ps. Because the 2923 cm^{-1} and 2938 cm^{-1} resonant Raman spectra are very close, they are detected at the same optical delay. Compared with the optical delay calibration method based on the excited Raman signals of standard samples and the sum-frequency generation in a nonlinear crystal, the temporal overlap estimation method proposed by us is wide wavelength suitability, flexible PCF change, quick troubleshooting capability and unlimited by optical power and phase-match. We hope that the temporal overlap estimation method proposed by us can realize the temporal overlap between pump pulse and Stokes pulse at once without any other adjustments or calibrations in wavelength-dependent optical delay adjustment system, such as the SSFS-based CARS system. More importantly, the dynamical closed-loop feedback time delay control can be expected in SSFS-based CARS system.

REFERENCES

[1] J.-X. Cheng and X. S. Xie, "Coherent anti-Stokes Raman scattering microscopy: Instrumentation, theory, and applications," *J. Phys. Chem. B.*, vol. 108, no. 3, pp. 827–840, 2004.

[2] E. O. Potma and X. S. Xie, "CARS microscopy for biology and medicine," *Opt. Photon. News*, vol. 15, no. 11, pp. 40–45, Nov. 2004.

[3] C. C. Moura, R. S. Tare, R. O. C. Oreffo, and S. Mahajan, "Raman spectroscopy and coherent anti-Stokes Raman scattering imaging: Prospective tools for monitoring skeletal cells and skeletal regeneration," *J. Roy. Soc. Interface*, vol. 13, no. 118, 2016, Art. no. 20160182.

[4] S. Osseiran, H. Wang, V. Fang, J. Pruessner, L. Funk, and C. L. Evans, "Nonlinear optical imaging of melanin species using coherent anti-Stokes Raman scattering (CARS) and sum-frequency absorption (SFA) microscopy," in *Proc. Novel Techn. Microsc. OSA*, 2017, Art. no. NS2C-3.

[5] S. You, Y. Liu, Z. A. Arp, Y. Zhao, E. J. Chaney, M. Marjanovic, and S. A. Boppart, "Intracellular imaging of docosanol in living cells by coherent anti-Stokes Raman scattering microscopy," *J. Biomed. Opt.*, vol. 22, no. 7, Jul. 2017, Art. no. 070502.

[6] A. M. Zheltikov, "Coherent anti-Stokes Raman scattering: From proof-of-the-principle experiments to femtosecond CARS and higher order wave-mixing generalizations," *J. Raman Spectrosc.*, vol. 31, nos. 8–9, pp. 653–667, 2000.

[7] Y. Zhang, C. S. Liao, W. Hong, K. Huang, H. Yang, G. Jin, and J. Cheng, "Coherent anti-Stokes Raman scattering imaging under ambient light," *Opt. Lett.*, vol. 41, no. 16, pp. 3880–3883, Aug. 2016.

[8] G. Saar, C. W. Freudiger, X. Xu, A. Huttner, S. Kesari, G. Young, and X. S. Xie, "Coherent Raman tissue imaging in the brain," *Cold Spring Harbor Protocols*, vol. 2014, no. 5, pp. 472–482, 2014.

[9] C. Cleff, A. Gasecka, P. Ferrand, H. Rigneault, S. Brasselet, and J. Duboissed, "Direct imaging of molecular symmetry by coherent anti-Stokes Raman scattering," *Nature Commun.*, vol. 7, May 2016, Art. no. 11562.

[10] P. Deladurantaye, A. Paquet, C. Paré, H. Zheng, M. Doucet, D. Gay, M. Poirier, J.-F. Cormier, O. Mermut, B. C. Wilson, and E. J. Seibel, "Advances in engineering of high contrast CARS imaging endoscopes," *Opt. Express*, vol. 22, no. 21, pp. 25053–25064, Oct. 2014.

[11] K. Hirose, T. Aoki, T. Furukawa, S. Fukushima, H. Niioka, S. Deguchi, and M. Hashimoto, "Coherent anti-Stokes Raman scattering rigid endoscope toward robot-assisted surgery," *Biomed. Opt. Express*, vol. 9, no. 2, pp. 387–396, Jan. 2018.

[12] M. Marrocco, "Time-domain coherent anti-Stokes Raman scattering in terms of the time-delayed Yuratich equation," *Opt. Lett.*, vol. 39, no. 16, pp. 4831–4834, Aug. 2014.

[13] G. O. Ariunbold and N. Altangerel, "Quantitative interpretation of time-resolved coherent anti-Stokes Raman spectroscopy with all Gaussian pulses," *J. Raman Spectrosc.*, vol. 48, no. 1, pp. 104–107, 2017.

[14] J.-X. Cheng, L. D. Book, and X. S. Xie, "Polarization coherent anti-Stokes Raman scattering microscopy," *Opt. Lett.*, vol. 26, no. 17, pp. 1341–1343, Sep. 2001.

[15] D. Oron, N. Dudovich, and Y. Silberberg, "Femtosecond phase-and-polarization control for background-free coherent anti-Stokes Raman spectroscopy," *Phys. Rev. Lett.*, vol. 90, no. 21, May 2003, Art. no. 213902.

[16] K. Hashimoto, J. Omachi, and T. Ideguchi, "Ultra-broadband rapid-scan Fourier-transform CARS spectroscopy with sub-10-fs optical pulses," *Opt. Express*, vol. 26, no. 11, pp. 14307–14314, May 2018.

[17] K. Hashimoto, M. Takahashi, T. Ideguchi, and K. Goda, "Broadband coherent Raman spectroscopy running at 24,000 spectra per second," *Sci. Rep.*, vol. 6, Feb. 2016, Art. no. 21036.

[18] F. Ganikhanov, C. L. Evans, B. G. Saar, and X. S. Xie, "High-sensitivity vibrational imaging with frequency modulation coherent anti-Stokes Raman scattering (FM CARS) microscopy," *Opt. Lett.*, vol. 31, no. 12, pp. 1872–1874, Jun. 2006.

[19] T. Ideguchi, S. Holzner, B. Bernhardt, G. Guelachvili, N. Picqué, and T. W. Hänsch, "Coherent Raman spectro-imaging with laser frequency combs," *Nature*, vol. 502, no. 7471, pp. 355–358, Oct. 2013.

[20] A. F. Pegoraro, A. Ridsdale, D. J. Moffatt, J. P. Pezacki, B. K. Thomas, L. Fu, L. Dong, M. E. Fermann, and A. Stolow, "All-fiber CARS microscopy of live cells," *Opt. Express*, vol. 17, no. 23, pp. 20700–20706, Nov. 2009.

[21] R. Xie, J. Su, E. C. Rentchler, Z. Zhang, C. K. Johnson, H. Shi, and R. Hui, "Multi-modal label-free imaging based on a femtosecond fiber laser," *Biomed. Opt. Express*, vol. 5, no. 7, pp. 2390–2396, Jul. 2014.

[22] E. C. Rentchler, R. Xie, R. Hui, and C. K. Johnson, "Two-frequency CARS imaging by switching fiber laser excitation," *Microsc. Res. Techniq.*, vol. 81, no. 4, pp. 413–418, 2018.

[23] P. Adany, D. C. Arnett, C. K. Johnson, and R. Hui, "Tunable excitation source for coherent Raman spectroscopy based on a single fiber laser," *Appl. Phys. Lett.*, vol. 99, no. 18, 2011, Art. no. 181112.

[24] F. R. Arteaga-Sierra, C. Milián, I. Torres-Gómez, M. Torres-Cisneros, G. Moltó, and A. Ferrando, "Supercontinuum optimization for dual-soliton based light sources using genetic algorithms in a grid platform," *Opt. Express*, vol. 22, no. 19, pp. 23686–23693, Sep. 2014.

[25] G. Agrawal, *Applications of Nonlinear Fiber Optics*. Amsterdam, The Netherlands: Elsevier, 2001.

[26] M. Born and E. Wolf, *Principles of Optics*. Oxford, U.K.: Oxford Univ., 1995.

[27] J. Su, R. Xie, C. K. Johnson, and R. Hui, "Single-fiber-laser-based wavelength tunable excitation for coherent Raman spectroscopy," *J. Opt. Soc. Amer. B.*, vol. 30, no. 6, pp. 1671–1682, Jun. 2013.

[28] T. Hellerer, A. Enejder, and A. Zumbusch, "Spectral focusing: High spectral resolution spectroscopy with broad-bandwidth laser pulses," *Appl. Phys. Lett.*, vol. 85, no. 1, pp. 25–27, Jul. 2004.

[29] I. Rocha-Mendoza, W. Langbein, and P. Borri, "Coherent anti-Stokes Raman microspectroscopy using spectral focusing with glass dispersion," *Appl. Phys. Lett.*, vol. 93, no. 20, 2008, Art. no. 201103.

[30] M. Müller and A. Zumbusch, "Coherent anti-Stokes Raman scattering microscopy," *Chem. Phys. Chem.*, vol. 8, no. 15, pp. 2156–2170, 2007.

[31] Y. Shen, A. A. Voronin, A. M. Zheltikov, S. P. O'Connor, V. V. Yakovlev, A. V. Sokolov, and M. O. Scully, "Picosecond supercontinuum generation in large mode area photonic crystal fibers for coherent anti-Stokes Raman scattering microspectroscopy," *Sci. Rep.*, vol. 8, no. 1, p. 9526, Jun. 2018.

YONGNING ZHANG received the B.S. and M.S. degrees from the Taiyuan University of Technology, Taiyuan, China, in 2013 and 2016, respectively. He is currently pursuing the Ph.D. degree in optical engineering with Tianjin University, Tianjin, China. His research interests include nonlinear fiber optics and coherent Raman scattering microscopy.

JUNFENG JIANG received the B.S. degree from the Southwest Institute of Technology, China, in 1998, and the M.S. and Ph.D. degrees from Tianjin University, Tianjin, China, in 2001 and 2004, respectively, where he is currently an Associate Professor. His research interests include fiber sensors and optical communication performance measurement.

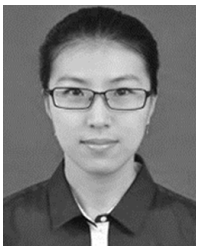

SHUANG WANG was born in Tianjin, China, in 1982. She received the B.S. degree from Shandong University, Shandong, China, in 2005, and the M.S. degree from Tianjin University, Tianjin, China, in 2007, where she is currently a Lecturer. Her research interests include optical fiber sensing and demodulation algorithm.

KUN LIU received the B.Eng., M.Eng., and Ph.D. degrees from Tianjin University, Tianjin, China, in 2004, 2006, and 2009, respectively, where he is currently an Associate Professor. His research interests include fiber physics and chemistry sensing systems.

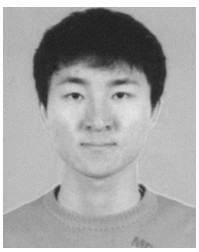

ZHE MA received the B.S. and M.S. degrees from the Taiyuan University of Technology, China, in 2012 and 2015 respectively. He is currently pursuing the doctorate degree in optical engineering with Tianjin University, Tianjin, China. His research interest includes distributed optical fiber sensing.

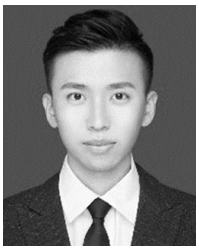

GAOFEI GU received the B.S. degree from the University of Electronic Science and Technology of China, Sichuan, China, in 2017. He is currently pursuing the M.S. degree in optical engineering with Tianjin University, Tianjin, China.

RONGQING HUI received the B.S. degree in microwave communications and the M.S. degree in lightwave technology from the Beijing University of Posts and Telecommunications, Beijing, China, in 1981 and 1988, respectively, and the Ph.D. degree in electrical engineering from Politecnico di Torino, Torino, Italy, in 1993. He is currently a tenured Associate Professor with the Department of Electrical Engineering and Computer Science, The University of Kansas, Lawrence.

TIEGEN LIU received the B.Eng., M.Eng., and Ph.D. degrees from Tianjin University, Tianjin, China, in 1982, 1987, and 1999, respectively. He is currently a Professor with Tianjin University. His research interests include photoelectric detection and fiber sensing. He is also a Chief Scientist of the National Basic Research Program of China.